Muon Capture in Gaseous Deuterium

A. Bertin* and A. Vitale

Istituto di Fisica dell'Università di Bologna and Istituto Nazionale di Fisica Nucleare, Sezione di Bologna, Bologna, Italy†

A. Placci and E. Zavattini

CERN, Geneva, Switzerland

(Received 3 July 1973)

We report the results of an experiment performed to measure the muon nuclear capture rate by free deuterons. The muons were slowed down in ultrapure gaseous hydrogen at 7.6 atm and 293 °K, containing 5% of deuterium. A special target was used, in which a system of gas proportional counters, working with the $(H_2 + D_2)$ gaseous mixture itself, was operating. Neutrons from the capture reactions were detected using liquid scintillation counters, and the γ-ray background was eliminated by pulse-shape discrimination. The experimental result is $\Lambda_{\exp} = (445 \pm 60) \sec^{-1}$, which is consistent with muon-electron universality and with the assumption that the nuclear capture proceeds from the doublet spin state of the μd muonic atoms. Combining the present experimental value with a previous result obtained with a liquid-hydrogen deuterated target, one obtains a ratio between the axial-vector and vector coupling constants given by $g_{A,\mu}/g_{V,\mu} = -1.35 \pm 0.1$.

I. INTRODUCTION

A. Purpose of Experiment

When a negative muon undergoes nuclear capture, the elementary process which takes place is the capture of the muon by a proton, according to the reaction

$$\mu^- + p \rightarrow n + \nu_\mu . \tag{1}$$

Process (1) is well described within the frame of the $V-A$ weak interaction coupling theory.[1-4] However, when muons are captured by high-atomic-number nuclei, a significant comparison between experimental results and theoretical predictions is complicated by the fact that we still do not have adequate knowledge of the effects of nuclear physics on the observable quantities for reaction (1).

The only process which can be studied, avoiding the complications due to nuclear physics, is the nuclear capture of muons by hydrogen, the rate of which can be calculated to an accuracy of about 5%.

Some measurements of the nuclear capture rate of muons by hydrogen were performed by several groups, using both liquid[5-8] and gaseous hydrogen[9] targets. In the first case, process (1) was taking place within $p\mu p$ molecular ions, whereas in the Bologna-CERN experiment[9] the reaction was observed starting from μp muonic atoms, i.e., in a system free of molecular effects.

The results obtained by these groups have made it possible to compare the rate of reaction (1) when it takes place in different total spin states of the muon-proton system, and they have been found in good agreement with the existing theory (see Table I). However, it should be kept in mind that the rate of process (1) is dependent on at least four parameters, i.e., the polar vector $(g_{V,\mu})$, axial-vector $(g_{A,\mu})$, induced pseudoscalar $(g_{P,\mu})$, and weak magnetism $(g_{M,\mu})$ coupling constants.[1-4] With the aim of determining these form factors only from experiments on reaction (1), more independent measurements are to be performed, the results of which are predicted by the theory to depend on different combinations of $g_{V,\mu}$, $g_{A,\mu}$, $g_{P,\mu}$, and $g_{M,\mu}$.

Despite our initial considerations, therefore, some experiments must be performed in the difficult field of muon capture by elements different from hydrogen.

A reasonable approach is, then, to consider muon capture by deuterons, i.e., the reaction

$$\mu^- + d \rightarrow n + n + \nu_\mu , \tag{2}$$

which is somewhat favored by the fact that, the deuteron wave function being sufficiently well known, the capture rate in the doublet spin state of the muon-deuteron system can be calculated to an accuracy of about 10% (more difficulties are met when calculating the same rate for the quartet state).

As was first pointed out by Überall and Wolfenstein,[10] moreover, reaction (1) is an almost pure Gamow-Teller process, due to the presence of two neutrons in the final state, and to the Pauli exclusion principle effects. Therefore, a measurement of the nuclear capture rate of muons by deuterons would allow us to get in particular a result which is more specifically related to the

TABLE I. Experimental results on the nuclear capture rate of muons by protons, and corresponding theoretical predictions.[a]

Authors	Type of H_2 target	Technique	$\Lambda_{M,\exp}$ (sec^{-1})	$\Lambda_{s,\exp}$ (sec^{-1})	$\Lambda_{M,\text{theor}}$ (sec^{-1})	$\Lambda_{s,\text{theor}}$ (sec^{-1})	$\Lambda_{t,\text{theor}}$ (sec^{-1})
Doede et al.[b]	liquid	bubble chamber	428 ± 85		493		
Bleser et al.[c]	liquid	counters	515 ± 85		522		
Bertolini et al.[d]	liquid	bubble chamber	450 ± 50		493		
Rothberg et al.[e]	liquid	counters	464 ± 42		522		
Alberigi Quaranta et al.[f]	gaseous	counters		651 ± 57		650	14.82

[a] The theoretical values reported in the table are taken from Ref. 4. Λ_s and Λ_t are capture rate of negative muons in the singlet and triplet spin state of the muon-proton system, respectively. $\Lambda_{M,\text{theor}}$ refers to nuclear captures of muons in the ortho state of the $p\mu p$ molecular ion.

[b] See Ref. 5.

[c] See Ref. 6.

[d] See Ref. 7.

[e] See Ref. 8.

[f] See Ref. 9.

axial-vector coupling constant $g_{A,\mu}$.

The latest theoretical predictions on the rate of process (2) are shown in Table II.[11-15] It is seen that the results of these different calculations are quite similar (within about 10%), except the one given by Cremmer.[12] However, the calculation by Cremmer contains some errors of sign[16] which affect the final value; if one corrects these errors, this result becomes very similar to the one given by Pascual et al.[13]

Figure 1 shows the spectrum of the neutrons emitted in reaction (2), as obtained by Wang.[11]

The first experimental result on this rate was given by the Columbia group (see Table II), which measured the nuclear capture rate of muons in $p\mu d$ molecular ions, formed by stopping negative muons in a target of liquid deuterated hydrogen. For such a molecular system, however, the theoretical prediction on the capture rate depends on the correct evaluation of the muon wave function overlap at the proton and at the deuteron. A way to avoid this difficulty would be to slow down muons in a low-density target (such as pure gaseous deuterium at the pressure of few atmospheres), so that the effective formation rates of μ molecules are sharply reduced. However, due to the presence of nuclear fusion reactions in the residual $d\mu d$ ions (as will be explained later), the experiment would be hardly feasible by stopping muons in pure deuterium.

Exploiting the high rate of the isotopic exchange reaction

TABLE II. Comparison between the experimental results and the latest theoretical predictions on the nuclear capture rate of muons by deuterons.

Authors	Experimental results (sec^{-1}) Λ_d	Theoretical values[a] (sec^{-1}) Λ_d	Λ_q	Λ_{st}
Bertin et al. (present experiment)	445 ± 60			
Wang[b]		334	15	121
Cremmer[c]		450[g]	30	170
Pascual et al.[d]		312.7	12	112
Truhlik[e]		376		
Wang et al.[f]	365 ± 96			

[a] Λ_d, Λ_q, and Λ_{st} correspond to nuclear capture of muons in the total spin state $F = \frac{1}{2}$, $F = \frac{3}{2}$, and in a statistical mixture of $F = \frac{1}{2}$ and $F = \frac{3}{2}$ states for the muon-deuteron systems.

[b] See Ref. 11.

[c] See Ref. 12.

[d] See Ref. 13.
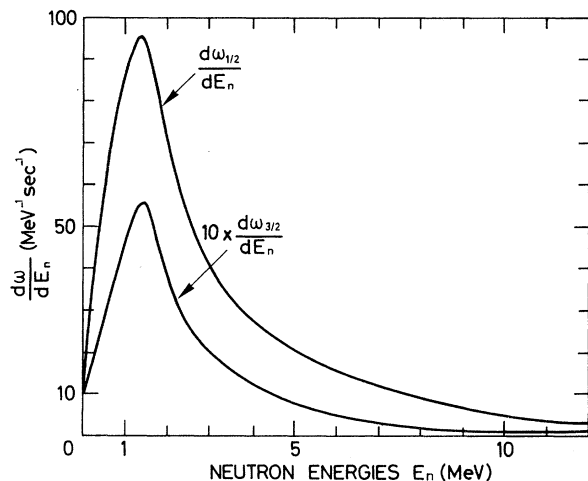
[e] See Ref. 14.

[f] See Ref. 15.

[g] See text.

FIG. 1. Calculated energy distribution for the neutrons emitted from muon capture by deuterons, as given by Wang (see Ref. 11). The two curves refer to capture processes in the doublet state $(d\omega_{1/2})$ and the quartet state $(d\omega_{3/2})$ of the hyperfine structure of the muon-deuteron system.

$$\mu p + d \rightarrow \mu d + p + 135 \text{ eV} \qquad (3)$$

(see Table III), [17-24] we have therefore performed a measurement of the rate of reaction (2) by stopping negative muons in ultrapure gaseous hydrogen at 7.6 atm and 293 °K, contaminated by 5% of deuterium. How the use of such a target makes the experiment possible will be discussed in detail in Sec. IB. The measurements were carried out identifying reaction (2) by detecting

TABLE III. Experimental results on the rates of some relevant μ-atomic and μ-molecular processes.[a]

Process	Rate	Experimental results[b] (10^6 sec^{-1})
$\mu p + p \rightarrow p \mu p$	λ_{pp}	$(2.55 \pm 0.18)^c$; $(1.89 \pm 0.20)^d$
$\mu d + d \rightarrow d \mu d$	λ_{dd}	$(0.75 \pm 0.11)^e$
$\mu p + d \rightarrow \mu d + p$	λ_e	$(1.43 \pm 0.13) \times 10^{4\,d}$; $(0.84 \pm 0.13) \times 10^{4\,f}$
$\mu d + p \rightarrow p \mu d$	λ_{pd}	$(6.82 \pm 0.25)^c$; $(5.8 \pm 0.3)^d$; $(1.8 \pm 0.6)^e$
$p \mu d \rightarrow {}^3\text{He} + \mu$	λ_{fb}	$(0.30 \pm 0.01)^d$
$\mu d + {}_Z Y \rightarrow \mu {}_Z Y + d$	$\lambda_{\mu d, Y}$	$\sim \frac{1}{2} (\lambda_{\mu p, Y})^g$
$\mu p + {}_Z Y \rightarrow \mu {}_Z Y + p$	$\lambda_{\mu p, Y}$	$5 \times 10^4 \div 5 \times 10^{5\,h}$

[a] For detailed discussions on the processes listed in the table, see Ref. 17.

[b] The quoted value for λ_{pp} refers to the density of liquid hydrogen. Similarly, the results for λ_e, λ_{dd}, and λ_{pd} refer to the rates at which the corresponding processes take place when the density of deuterium molecules is equal to 2.11×10^{22} molecules cm^{-3}, and the values given for $\lambda_{\mu p, Y}$ and $\lambda_{\mu d, Y}$ refer to a density of the ${}_Z Y$ elements equal to 2.11×10^{22} molecules cm^{-3}.

[c] See Ref. 18.
[d] See Ref. 19.
[e] See Ref. 20.
[f] See Ref. 21.
[g] See Refs. 23 and 24.
[h] See Ref. 22.

one of the outgoing neutrons. Except for some modifications, the apparatus was the same as that used by Alberigi Quaranta et al.[9] to measure the nuclear capture rate of muons in gaseous hydrogen. The present measurement was conceived with the following purposes:

(i) to observe process (2) starting from μd muonic atoms, i.e., in a system free of molecular complications;

(ii) to improve the accuracy in the experimental results, since the theoretical predictions now seem to be well founded;

(iii) to get further information on $g_{A,\mu}$ from a muon capture experiment, since the chief results on this form factor are given so far by the value of the branching ratio $(\pi \rightarrow \mu + \nu)/(\pi \rightarrow e + \nu)$ (Ref. 25) and of the muon nuclear capture rate in ${}^{12}\text{C}$.[26,27]

Preliminary results of the present experiment have already been reported.[28] Some auxiliary measurements were performed later[21,29] to get a more direct control of the correction to the experimental results. Therefore, the final value given in the present paper corresponds to the analysis of the whole set of collected events (almost twice those examined for the preliminary work), and to a more direct evaluation of the corrections involved.

B. The Method

When nuclear capture experiments are performed by slowing down muons in hydrogen or deuterium, the system in which reactions (1) and (2) take place is strictly dependent on the atomic and molecular processes which muons undergo in these media. One slowed muon forms at first an excited μp (H_2 target) or μd (D_2 target) muonic atom, which promptly decays to its lowest orbital level. The general features of the processes which the muonic atoms undergo in both gases are somewhat similar (see Tables III and IV)[30-35]; in the case of pure deuterium, however, the consequences of the molecular phenomena turn out to be much more critical, and prohibitive for the present purposes, as will be seen in the following.

The neutral μd atom, in fact, diffusing throughout the deuterium, may get bound in a $d \mu d$ molecular ion, according to the process

$$\mu d + d \rightarrow d \mu d . \qquad (4)$$

Contrary to what happens in a hydrogen target after the corresponding reaction

$$\mu p + p \rightarrow p \mu p , \qquad (5)$$

the $d \mu d$ system can undergo, with high probability, the fusion processes

TABLE IV. Some theoretical and experimental results on the scattering cross sections for μp and μd atoms.

Process	Cross section	Experimental results (10^{-21} cm^2)	Theoretical predictions (10^{-21} cm^2)
$\mu p + p \rightarrow \mu p + p$	σ_0 [a]	(7.6 ± 0.7) [b]	8.2 [c]; 1.2 [d]; 2.5 [e];
$\mu d + d \rightarrow \mu d + d$	$\sigma_{\mu d + d}$	(55 ± 20) [b]; (150 ± 50) [f]	350 [c]; 330 [d]; 180 [e];
$\mu d + p \rightarrow \mu d + p$	$\sigma_{\mu d + p}$	$(0.8^{+0.3}_{-0.4})$ [g]	~ 1 [c]
$\mu d + {}_Z Y \rightarrow \mu d + {}_Z Y$	$\sigma_{\mu d + Y}$	(1200 ± 300) [g]; $> 10^6$ [h]	~ 1000 [c]

[a] This cross section refers to colliding μp atoms in the singlet spin state.
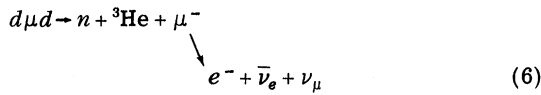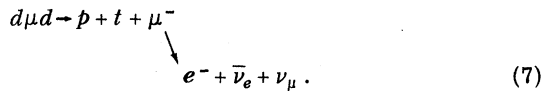[b] See Ref. 30.
[c] See Ref. 31.
[d] See Ref. 32.
[e] See Ref. 33.
[f] See Ref. 34.
[g] See Ref. 35.
[h] See Ref. 23. The reported value refers to the case $_Z Y$ = xenon.

$$d\mu d \rightarrow n + {}^3\text{He} + \mu^-$$
$$\searrow$$
$$e^- + \bar{\nu}_e + \nu_\mu \qquad (6)$$

and

$$d\mu d \rightarrow p + t + \mu^-$$
$$\searrow$$
$$e^- + \bar{\nu}_e + \nu_\mu \ . \qquad (7)$$

The neutrons emitted in reaction (6) have an energy of 3.3 MeV, so that they may be exchanged for neutrons coming from process (2) (see Fig. 1).

One can easily see, therefore, that reaction (6) constitutes a serious source of neutron background. The neutron yield from this reaction per formed μd atom in a target of pure deuterium is, in fact, given by

$$N_f = \frac{\phi \lambda_{dd}}{\lambda_0 + \lambda_{dd}} F , \qquad (8)$$

where λ_0 is the free muon decay rate ($\lambda_0 = 4.54 \times 10^5 \text{sec}^{-1}$), λ_{dd} is the rate for reaction (4) (see Table III), ϕ is the ratio between the density of deuterium at the chosen pressure and a density of atoms $\rho_0 = 4.22 \times 10^{22}$ atoms cm^{-3}, and F is that fraction of $d\mu d$ ions which disappear through process (6).[20,36]

N_f was measured by Dzhelepov et al.[20] in a diffusion chamber filled with deuterium at different pressures and known admixtures of methyl and propyl, at a temperature between 250 °K and 275 °K. From the results given by these authors, one gets in a pure deuterium target, even at a pressure of about 7 atm, N_f of the order of 10^{-2}.

Since the neutron yield due to muon capture in μd muonic atoms is expected to be of the order of 10^{-3} (see Table II), this fact means, as was anticipated, that a muon nuclear capture experi-

ment becomes hardly feasible by stopping muons in a target of pure gaseous deuterium: In fact, the number of neutrons emitted from process (6) would be much larger than the number of neutrons emitted from process (2).

A first step in the right direction is to slow down muons in a gaseous mixture of hydrogen with a small contamination of deuterium, which is the method followed for the present measurement. In this case, the muons which slow down in the target (7.6 atm hydrogen plus 5% deuterium) initially form μp muonic atoms. Owing to the high rate of reaction (3) and to the chosen deuterium concentration, the muons are transferred to deuterium within a time which is short compared to the muon decay rate λ_0. In particular, assuming for the rate λ_e of reaction (3) the recent result obtained by Bertin et al.[21] at room temperature, one gets that the μp system has a mean lifetime of about 220 nanoseconds in the present experimental conditions. On the other hand, the formation of $d\mu d$ molecules, which proceeds at an effective rate $\phi \lambda_{dd}$, is sharply reduced because deuterium is present in the target only at a low partial pressure. Most of the stopped muons, therefore, should decay when they are still bound in μd muonic atoms.

In this case, N_f is given by

$$N_f = \frac{\phi \lambda_{dd}}{\lambda_0 + \phi \lambda_{dd} + \psi \lambda_{pd}} F , \qquad (9)$$

where ψ is the ratio between the hydrogen density at 7.6 atm and ρ_0, and λ_{pd} is the formation rate for $p\mu d$ molecular ions. From the results by Dzhelepov et al.[20] on λ_{dd} and λ_{pd} (see Table III), in this case one gets $N_f \cong 4 \times 10^{-4}$.

A factor of 2 is actually gained in favor of muon capture by deuterons, because this reaction

produces two neutrons in the final state. Further-more, as will be seen in Sec. II, the apparatus used for the present measurement includes a slow anticoincidence system for charged particles, so that, owing to the presence of the delayed decay electron in the final state of reaction (6), this process is, to a large extent, in anticoincidence with the apparatus itself.

The corresponding background counts are then limited to a small contribution, which will be taken into account in Sec. III.

As for the other processes listed in Table III, it should be noted that the $p\mu d$ molecular ions, following the reaction

$$\mu d + p \rightarrow p\mu d, \qquad (10)$$

are formed in the present case for about 4% of the initial μd's. In this system, a fusion reaction leading to a ^{3}He nucleus can also take place, but this process does not contribute to the neutron counting rate, except for a small correction due to the nuclear capture of the muon by the pro-duced ^{3}He itself. Also the nuclear captures of muons by protons and deuterons in the $d\mu d$ and $p\mu d$ ions give rise to a small contribution; all of these can easily be taken into account.

One more important difference between the slowing-down processes concerning μp and μd atoms is the fact that the depolarization processes occurring through scattering of the μd system against the surrounding molecules have not yet been completely clarified. Here one must re-member that the $V-A$ character of reactions (1) and (2) implies that the rate of these reactions is strongly dependent on the total spin state of the muon-nucleon system (see Tables I and II). To achieve a significant comparison between the present experimental results and the theoretical predictions, it is, then, important to know exactly what is the total spin of the μd system in which the nuclear capture process takes place.

The μd atoms can exist in two hyperfine struc-ture states, i.e., the $F = \frac{1}{2}$ doublet state and the $F = \frac{3}{2}$ quartet state, F being the total spin of the μd system. The energy difference between these two levels is[37]

$$\Delta E = 0.046 \text{ eV}. \qquad (11)$$

The μd muonic atoms are initially formed in a statistical mixture of doublet and quartet states, and the evolution of the spin states is conditioned by the scattering against the surrounding mole-cules.

In the present experimental conditions, the μd atoms are initially produced with a kinetic energy of 45 eV because of reaction (3), and are slowed down both by scattering against deuterium mole-cules,

$$\mu d + d \rightarrow \mu d + d \qquad (12)$$

and against hydrogen ones,

$$\mu d + p \rightarrow \mu d + p. \qquad (13)$$

In fact, even if the deuterium is present in the target only at a small concentration, each of the processes (12) and (13) becomes dominant one upon the other, according to the energy of the μd system (see Fig. 2).[31]

As for the final spin state of the scattered μd atoms, it has been shown[32,38] that depolarization from the quartet to the doublet state through the *jump mechanism* of the muon from one deuteron to the other in process (12) should occur in our conditions at a negligible rate. On the other hand, calculations on the collision cross section for process (13) have been done by Cohen et al.[31] and by Belyaev et al.[39] These authors, however, do not take into account the hyperfine interaction between the μd atom and the proton in process (13). We must then conclude that no information is available on how the total spin state of the μd atom evolves in time in our experimental condi-tions, although it has been advanced by us[28] that the hyperfine mixing in the colliding $(\mu d + p)$ sys-tem may lead to a substantial — if not total — con-
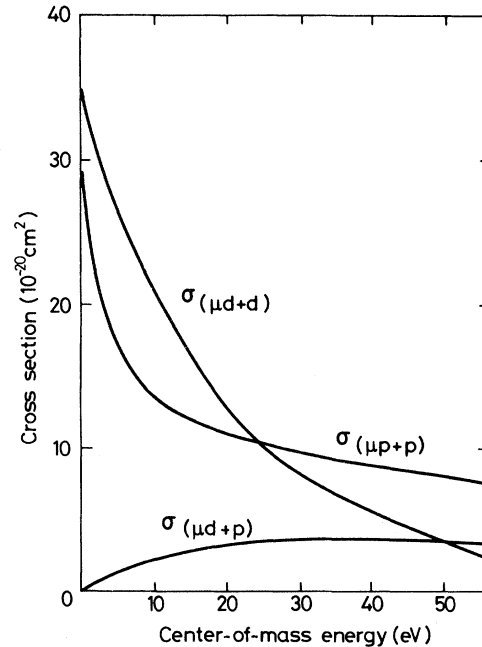
FIG. 2. Theoretical values of the cross sections for the scattering processes $\mu p + p \rightarrow \mu p + p$, $\mu d + d \rightarrow \mu d + d$, and $\mu d + p \rightarrow \mu d + p$, as given by Cohen (see Ref. 31).

version of the μd atoms to the doublet state in reaction (13).

C. Background Problems

In the present experiment, the neutrons were detected by liquid scintillation proton-recoil counters.[40] Pulse-shape discrimination was used to eliminate the background of γ rays.

As for the neutron counting rate, it has to be mentioned that, besides the spurious events due to fusion reactions in the $d\mu d$ molecular ions, which are characteristic of muon capture in deuterium, the following background channels had to be minimized:

(i) neutrons due to the nuclear capture of muons by impurity atoms $_ZY$ (Z being the atomic number) contained in the gaseous mixture;

(ii) neutrons due to nuclear capture of muons stopping directly in elements other than hydrogen, which were part of the target itself;

(iii) neutrons coming from $N(\gamma, n)N'$ reactions on the materials surrounding the apparatus; these were specially due to the γ rays generated by the bremsstrahlung of the muon decay electrons;

(iv) neutrons due to the nuclear capture of muons transferred to the atoms of the stainless steel wall and wires (see below) of the container by diffusing μd atoms;

(v) accidental neutrons.

It has to be pointed out that the neutrons coming from points (iii) and (iv) are specially misleading, since their time distribution is quite similar to that of neutrons coming from reaction (2). All the background channels (i)–(v) were already met while measuring the muon nuclear capture rate in gaseous hydrogen, so that it was possible to quench them by using almost the same apparatus.

The background channels due to point (i) are chiefly due to the high rates of the transfer processes[22–24]

$$\mu p + _ZY \rightarrow \mu_ZY + p \tag{14}$$

and

$$\mu d + _ZY \rightarrow \mu_ZY + d , \tag{15}$$

and to the fact that the nuclear capture rate of muons by elements increases roughly as Z^4.[41] The corresponding spurious events were eliminated by purifying both the hydrogen and the deuterium gases by a palladium filter[42] before entering the target. The used hydrogen (protium) (Ref. 43) contained, on the other hand, less than 3 ppm (parts per million) of deuterium.

The neutrons due to all the other sources were reduced mainly by the operation of a series of anticoincidence wire-proportional counters, work-
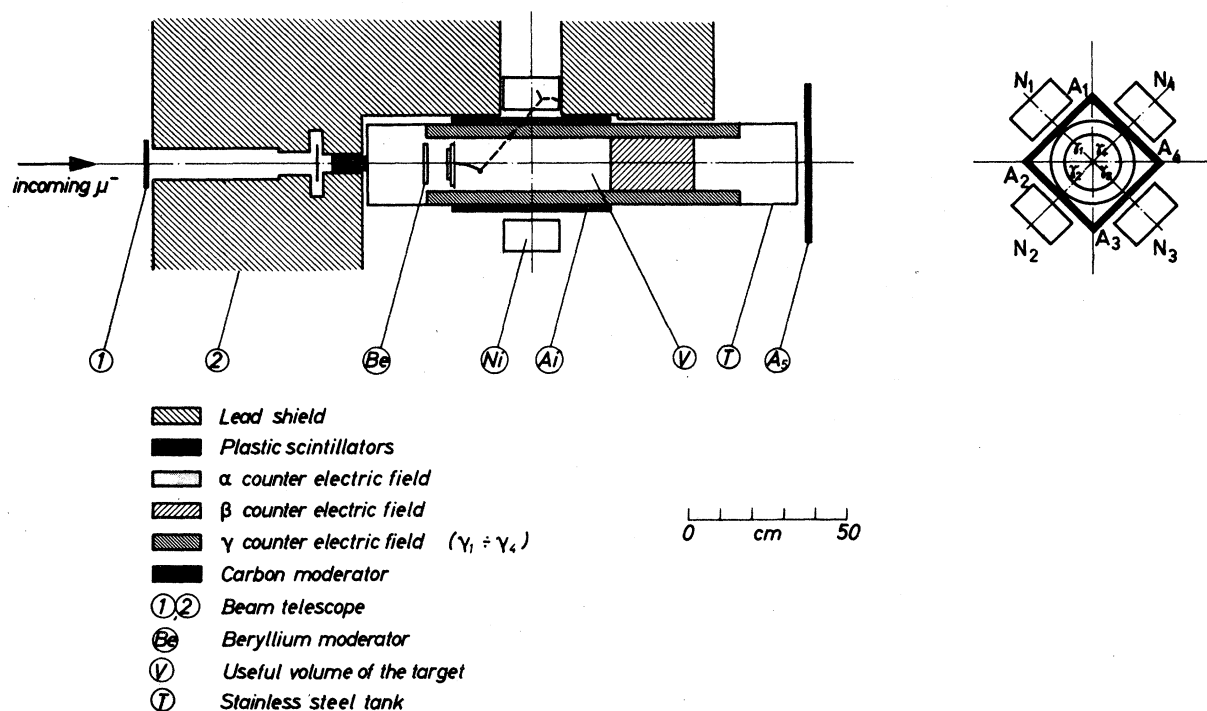

FIG. 3. Simplified scheme of the experimental arrangement used to measure the nuclear capture of negative muons by free deuterons in a deuterated hydrogen gaseous target.

ing with the gaseous mixture itself as a filling gas. Those due to point (ii) were further rejected by accepting only those events which were delayed by more than 500 nanoseconds with respect to the incoming muon. The target and the surrounding materials were exclusively made of high-atomic-number elements (Pb, Fe), except for some PTFE insulators, which were shielded from the incoming muons by regions of the anticoincidence proportional counters (see Figs. 3 and 4).

As a final comment, one should remember that, apart from the difficulties in the theoretical interpretations of the nuclear and molecular effects,

the neutrons emitted in reaction (2) have a continuous energy distribution (see Fig. 1) with a peak in a very-low-energy region (~ 1.4 MeV).

II. EXPERIMENT

A. Detection of Nuclear Capture Events

The experimental value Λ_{exp} for the nuclear capture rate of negative muons by deuterons is defined in our case by
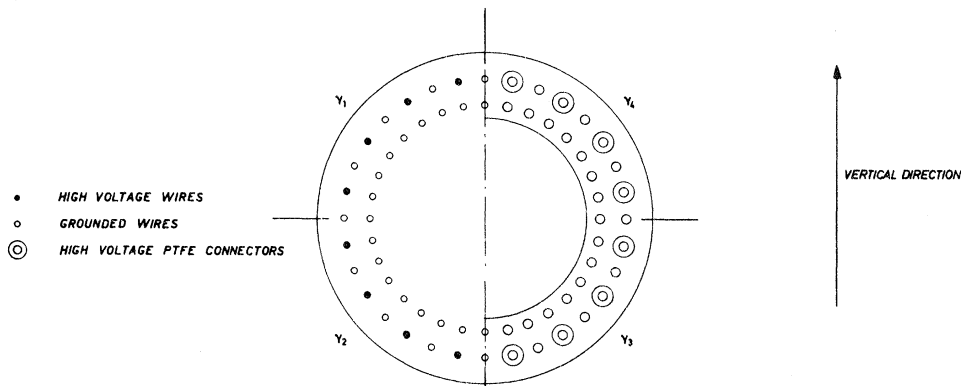
$$\Lambda_{exp} = (\lambda_0 N)/(ME) , \qquad (16)$$

where N is the number of neutrons due to process

① α COUNTER
② A γ COUNTER HIGH VOLTAGE ELECTRODE
③ γ COUNTER GROUNDED ELECTRODES
④ β COUNTER HIGH VOLTAGE ELECTRODE
⑤ GUARD ELECTRODES FOR β COUNTER
⑥ NYLON INSULATING WIRE
⑦ SILVER SUPPORTING WIRE
⑧ STAINLESS STEEL CONTAINER
⑨ PTFE INSULATING SUPPORTS
⑩ END OF THE USEFUL VOLUME V

(a)

• HIGH VOLTAGE WIRES
○ GROUNDED WIRES
◎ HIGH VOLTAGE PTFE CONNECTORS

(b)

FIG. 4. Schematic drawing of the special target: (a) side view of the container and of the complete structure of wire proportional counters; (b) geometry of the wires of counter γ and of the four γ_i sections.

(2) detected by the apparatus, M is essentially equal to the number of formed μd systems for which the muon decayed before any molecular process took place, and E is the over-all efficiency of the apparatus for detecting at least one of the neutrons emitted in reaction (2).

The quantity M was determined by looking at the yield of the decay electrons coming from the muons stopped in the gaseous mixture. The electrons were detected by systems of counters (*electron telescopes*) which also included the liquid scintillation counters used as neutron detectors. The over-all efficiency of the apparatus for counting electrons, as well as the quantity E in Eq. (16), are to be calculated.

A simplified scheme of the apparatus used for the experiment is shown in Fig. 3. The target, the operation of the special proportional counters, and the electronics were described in detail elsewhere.[9,40,44] We shall only recall here their main characteristics.

B. The Target

The cylindrical vessel containing the gaseous mixture was 260 mm in diameter and 1352 mm long. It had a reduced thickness both in the front flange (1 mm) and in that part of the side surface which was facing the neutron counters (2.5 mm). Figure 5 shows a scheme of the filling system used to let the various gases into the container. This was built under severe requirements of pressure and vacuum tightness (25 atm and 10^{-7} Torr), and in such a way that it could tolerate high-voltage power supplies (30 kV) without being subject to electrostatic discharges. (High volt-

ages were requested for the operation of the proportional counters.[44])

Three different stainless steel wire-proportional counters were operating inside the vessel (see Figs. 3 and 4):

(a) A plane-structure grid (α counter) was placed in front of the entrance window, and was operating in fast coincidence to define the incoming beam (total jitter: 0.5 microseconds).

(b) A peripheral structure of 16 quasicylindrical wire-proportional counters (γ counter) defined an electric field along the internal side surface of the container, and was producing anticoincidence signals for each charged particle arriving at a distance less than 4.4 cm from the side surface itself. This counter was divided into four sections (γ_1, γ_2, γ_3, γ_4), each of which could operate independently from the others. Each γ_i was facing one of the N_i neutron counters (see Fig. 3).

(c) A cylindrical counter (β counter) was situated in the back of the container, and had the same anticoincidence function as the γ counter with respect to the back wall of the tank. The time fluctuations of the signals coming from the β and γ counters were of the order of 10 microseconds.

A signal $[\alpha, \sim(\beta+\gamma)]$ (here $\sim$ means "not") defined a muon stopping in the useful volume V, which was delimited essentially by the electric fields of the proportional counters and only by a few extremely thin wires (100 microns in diameter). V was a cylinder 491 mm long and 172 mm in diameter.

The dimensions of the β and γ counters were chosen in such a way that the muons forming μd atoms within the V volume certainly decayed
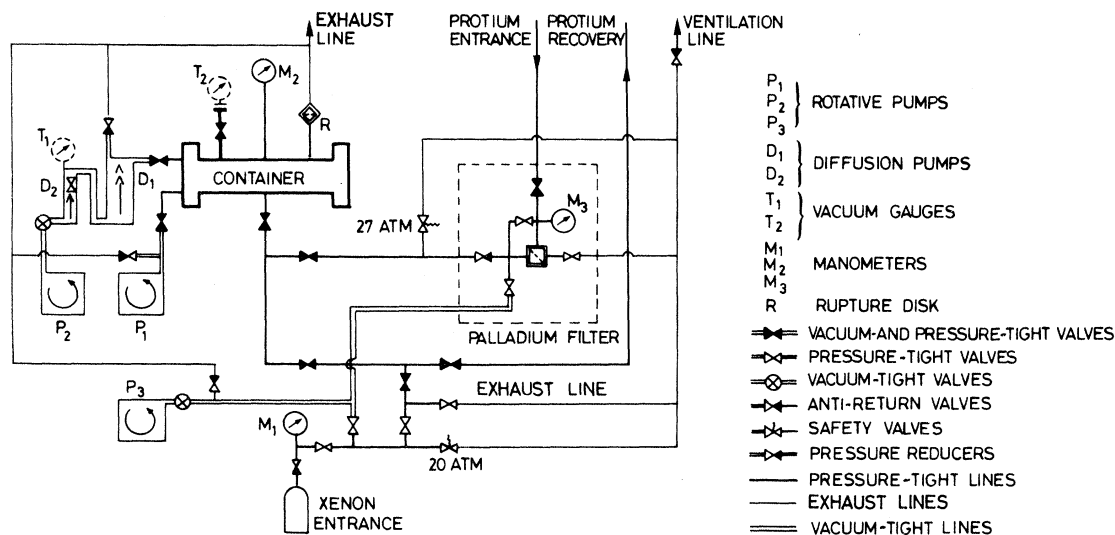

FIG. 5. Scheme of the gas-filling circuit.

before the μd atoms could diffuse up to the container walls. In this way, the neutron background, due to the possible transfer of muons to the atoms of the wall, was drastically cut off.

We also calculated that the β and γ proportional counters, working in slow anticoincidence, actually reduced the neutron background due to the fusion reaction in the $d\mu d$ system [see Eq. (6)] by a factor larger than 85%, by detecting the corresponding muon decay electron (the residual 15% is due to the electrons escaping through the α grid).

It is also worthwhile mentioning that it was possible[44] to control that the gaseous mixture in the container remained pure to better than 1 ppm over a period of one day. On the other hand, no significant difference was observed in the behavior of the proportional counters when the gaseous mixture ($H_2 + 5\%$ D_2) was used instead of pure protium.

C. The Neutron Detectors

The four proton-recoil neutron counters N_i were disposed symmetrically around the target (see Fig. 3), and placed in cylindrical cavities made in lead shielding blocks. A layer of paraffin covered the whole apparatus.

To improve the energy resolution—in view of the mentioned low-energy distribution of the neutrons coming from process (2), and in order to better subtract the 5.2-MeV neutrons coming from process (1)—the neutron counters used for the present experiment had smaller size than for the hydrogen one.[40] They were made of NE-213 (Ref. 45) liquid scintillator, contained in cylindrical glass cells 4 in. long and 5 in. in diameter. Each cell was viewed directly by a 54 AVP photomultiplier.

The pulse-shape discrimination was obtained by a simplified technique, using only standard electronics, and keeping in mind the requirements of having a neutron-γ discrimination effective over a wide interval of energies, compatible with a good energy resolution.

Figure 6 shows how the pulses corresponding to neutrons and γ rays distributed themselves on a two-dimensional display of the amplitudes (AN_i) versus tail (TN_i) signals from the N_i counters. [AN_i was proportional to that part of the scintillation pulse contained between its beginning (t_0) and about 50 nanoseconds after; TN_i corresponds to the integration of that part of the signal contained between 60 and 200 nanoseconds after t_0 (Ref. 40)].

The optimization of these figures was achieved for each counter using a Po-Be source, which was also used to check the stability of the position of
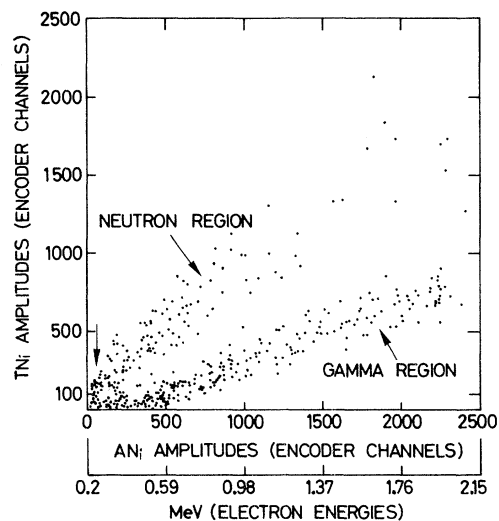

FIG. 6. A typical two-dimensional plot of the AN_i and TN_i amplitudes as released by the ADC (encoders) connected to the neutron counters. The arrow on the horizontal scale shows a reference cut of 0.25 MeV below which the neutron-γ discrimination is poor. For the data analysis, a minimum lower cut of 0.35 MeV was used.
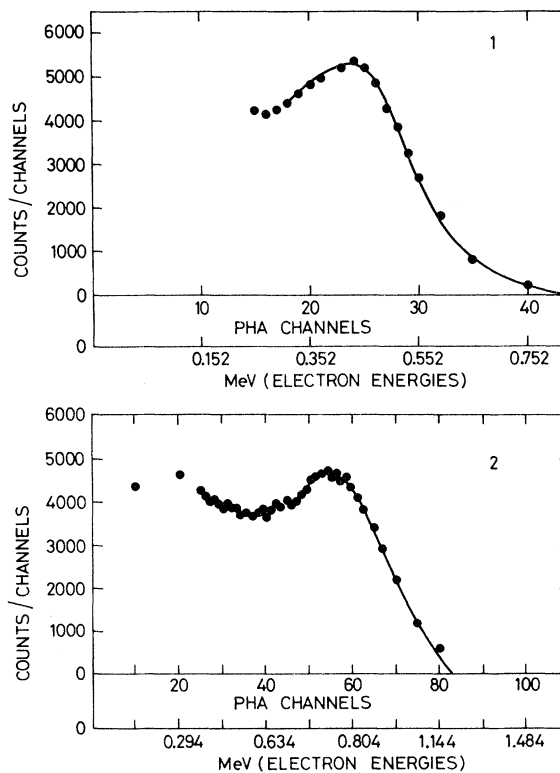

FIG. 7. Typical spectra obtained with γ-radioactive sources by the neutron detectors. The points on the figure are experimental data, whereas the full lines are the result of a χ^2 fit of the calculated distributions with the experimental points: (1) ^{137}Cs source; (2) ^{60}Co source.

the neutron and γ regions shown in Fig. 6. In the worst case, about 2% of the detected γ rays gave their representative point within their neutron region at 0.25 MeV (electron equivalent energy); at higher energies, of course, such contamination became negligible.

The energy scale and resolution of the N_i counters were periodically measured by means of radioactive sources supplying γ rays of suitable energies (^{60}Co and ^{137}Cs). The spectra obtained from these sources were then analyzed by a Monte Carlo calculation, which supplied the electron energy scale and the energy resolution (see Fig. 7). In the chosen working conditions, the average energy resolution of the N_i neutron counters was about 9% at 3 MeV (electron equivalent energy).

D. The Fast Counters

Two fast plastic scintillators (counters 1 and 2, see Fig. 3) were measuring the incoming beam. Four other plastic scintillators A_i were disposed around the target as the four sides of a square box, between the target and the corresponding N_i

detector. Each A_i was used either in fast coincidence with the corresponding N_i counter (*electron selection*) or in fast anticoincidence with it (*neutral selection*). Another plastic scintillator A_5 was put after the back flange of the gaseous target to be used in fast anticoincidence with the counters defining the stopping beam.

E. The Measurements

The experiment was performed at the muon channel of the CERN 600-MeV Synchrocyclotron, which was operated with a duty cycle of about 30%. The 130-MeV/c negative muon beam was focused towards a zone of the experimental hall (see Fig. 8) where previous measurements had shown that the local background was sufficiently low to allow the capture experiments.

The muons were collimated by a lead collimator, having a diameter of 6 cm in its last section. A polyabsorber slowed down the muons before they entered the target. A beryllium moderator, 1 cm thick, was used as the last absorber to minimize losses due to multiple scattering. The beryllium was placed inside the gaseous target, at about

SHIELDING WALLS
F GAS CIRCUITRY (RECYCLING,FILLING AND FIRST PURIFICATION)
E POSITION OF THE ELECTRONICS
BM BENDING MAGNET
FQ FOCUSSING QUADRUPOLES
C LAST LEAD COLLIMATOR (∅6cm)
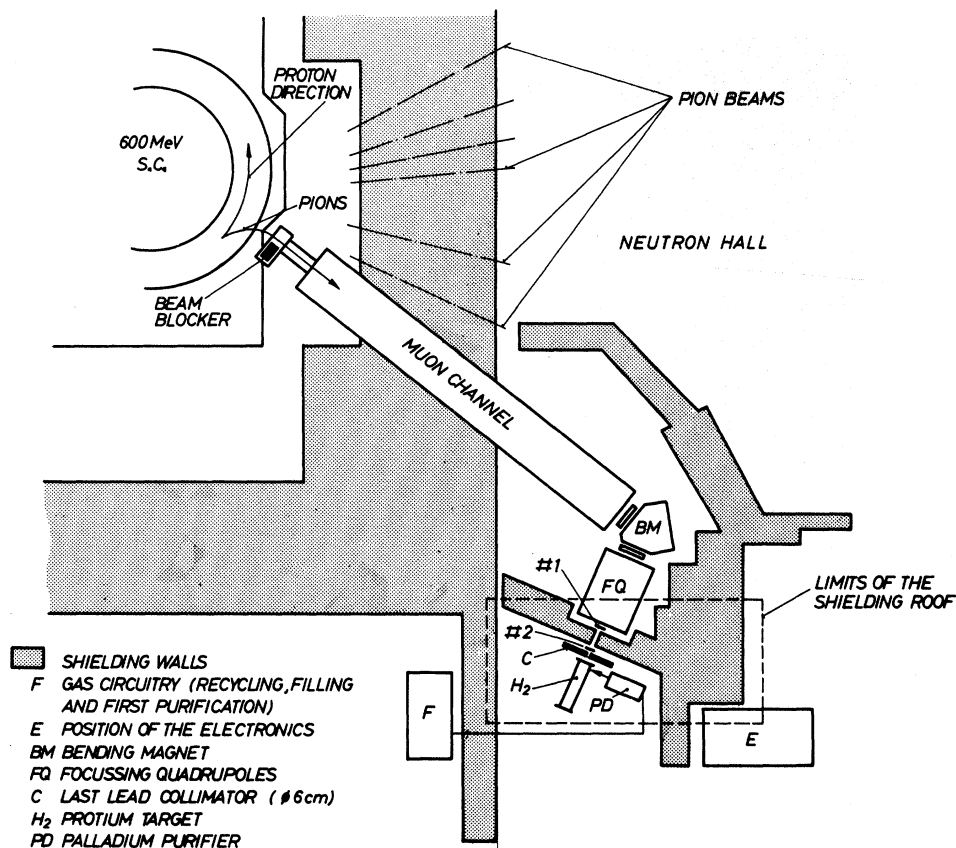H₂ PROTIUM TARGET
PD PALLADIUM PURIFIER

FIG. 8. Over-all view of the experimental layout on the Synchrocyclotron floor, showing beam optics and shielding arrangements.

7 cm before counter α. The thickness of the carbon moderator was optimized by looking at the number of decay electrons detected by the electron telescopes in the *electron selection* condition. A typical range curve obtained in this way is shown in Fig. 9. Setting the threshold of counter α at a proper level proved to be of major importance to select those particles which were likely to stop in the useful volume V of the target.[24]

Figure 10 shows a simplified diagram of the electronics. The beam entering the target was monitored by the $(1,2)$ fast coincidence of the plastic scintillators 1 and 2 (MONITOR coincidence). The stopping time of a muon in the useful volume V was defined by a MUSTOP anticoincidence signal $[1,2,\alpha,\sim(\sum A_i,\beta,\gamma)]$ (here $\sim$ means "not"). Table V shows the main counting rates of significance with regard to the beam conditions.

It should be noted here that the MUSTOP anticoincidence contained some fast signals (from the plastic scintillators) and some slow ones (especially from counters β and γ). The latter were accepted in the MUSTOP anticoincidence within a large gate, in order to be able to anticoincide also the decay electrons from the muon in the final state of the fusion reaction (6).

The MUSTOP signal opened a gate 10 microseconds long, waiting for a signal coming from
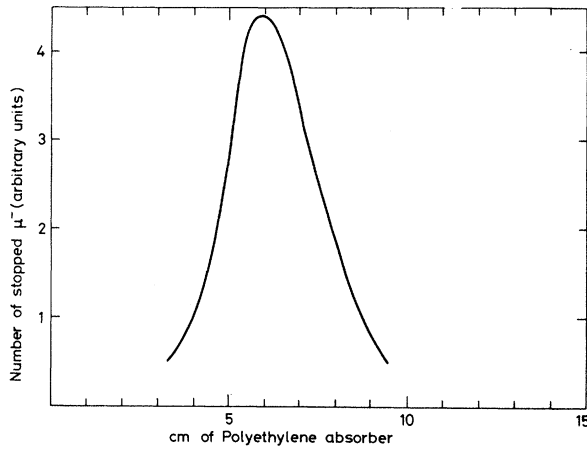

FIG. 9. Typical range curve obtained for the present measurements.

one of the N_i counters into the TRIGGER coincidence. The length of the gate was chosen in order to accept also delayed accidentals.

Each N_i counter always coincided with the corresponding A_i in a fast coincidence circuit (A_i, N_i) *(electron telescope)*. The data output was achieved in two different ways.

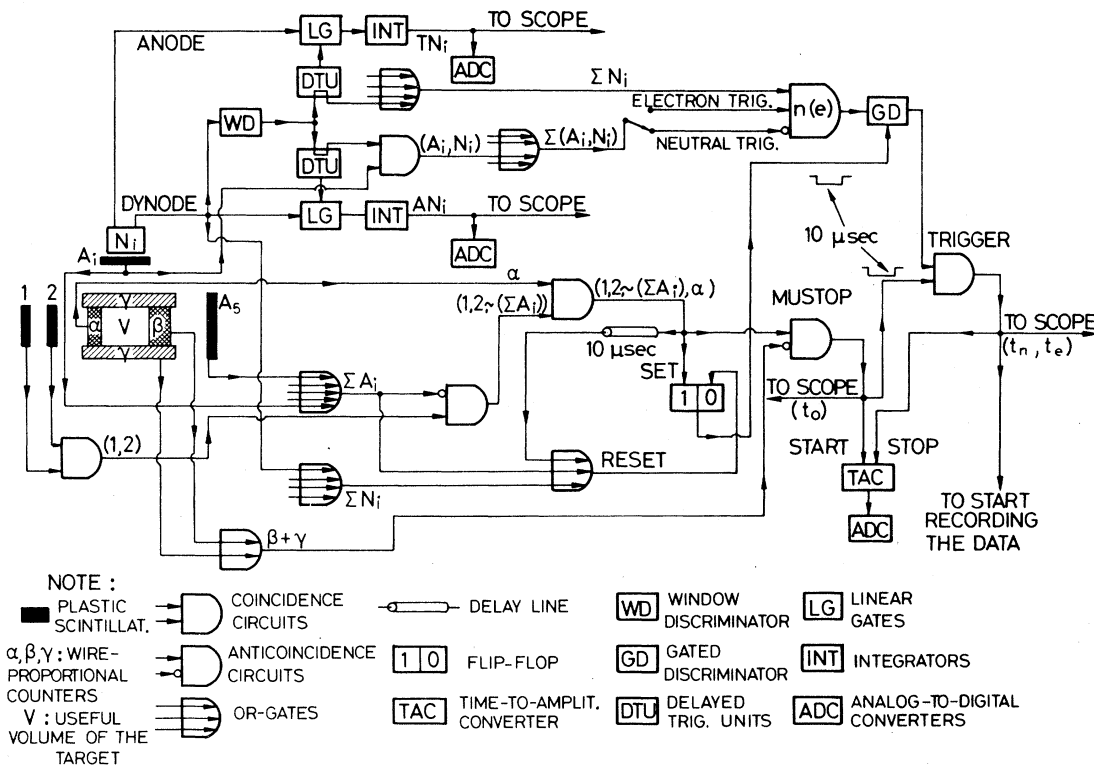(i) *Neutral trigger.* This was defined by the TRIGGER coincidence signal in the following con-

FIG. 10. Simplified block diagram of the electronics.

TABLE V. Typical counting rates of the main beam-monitoring circuits[a] in the present experiment.

MONITOR (particles/sec)	$(1, 2, \alpha)$ coincidence (particles/sec)	MUSTOP (particles/sec)
15 000	2000	30

[a]See Fig. 10.

ditions:

(a) The pulses coming from the N_i neutron counters were properly discriminated in amplitude by window discriminators;

(b) the output of the window discriminators was in *anticoincidence* with the signals coming from the (A_i, N_i) electron telescopes;

(c) the gate coming from the MUSTOP signal was closed immediately after the passage of the N_i signal, or could be closed at any time by a second MONITOR signal, or finally by a pulse coming from any of the A_i counters.

In this case, the TRIGGER signal started to record the time (t_n), the amplitude (AN_i), and the tail (TN_i) of the pulse coming from N_i in digitized form. The same information was photographed on the tracks of two double-beam oscilloscopes, 55 microseconds long, together with the signals from counters β and γ and other quantities of interest (see Fig. 11). The analysis of the pictures then made it possible to increase the anti-coincidence efficiency of the proportional counters by recognizing those cases in which the electronic

anticoincidences had failed because of the large time jitter of counters β and γ. A system of four lamps was displayed on the pictures, to associate them to the corresponding digitized output.

(ii) Electron trigger. This was defined by the TRIGGER signal in the following conditions:

(a) The upper thresholds of the discriminators following the N_i neutron counters were removed;

(b) the (A_i, N_i) electron telescopes were put in *fast coincidence* with the corresponding N_i counter;

(c) the pulses coming from the A_i counters were not allowed to switch off the gate opened by the MUSTOP signal.

The circuitry was arranged in this case in such a way that it worked with only one electron telescope at a time. This was done by disconnecting the γ_i section of the γ proportional counter which was facing the (A_i, N_i) telescope that was counting (see Fig. 3). The trigger signal, moreover, did not drive the two oscilloscopes, but still started recording the time interval between the MUSTOP (t_0) and the time of the (A_i, N_i) signal (t_e) in digitized form.

Special care was taken to ensure that the origin of the time intervals should be the same both in the *neutral* and in the *electron trigger* conditions. The output pulses of the N_i counters were accepted only after a fixed delay of 500 nanoseconds after the MUSTOP signal in both cases.

The TN_i pulses, essential for the neutron-γ discrimination, were not used in the trigger
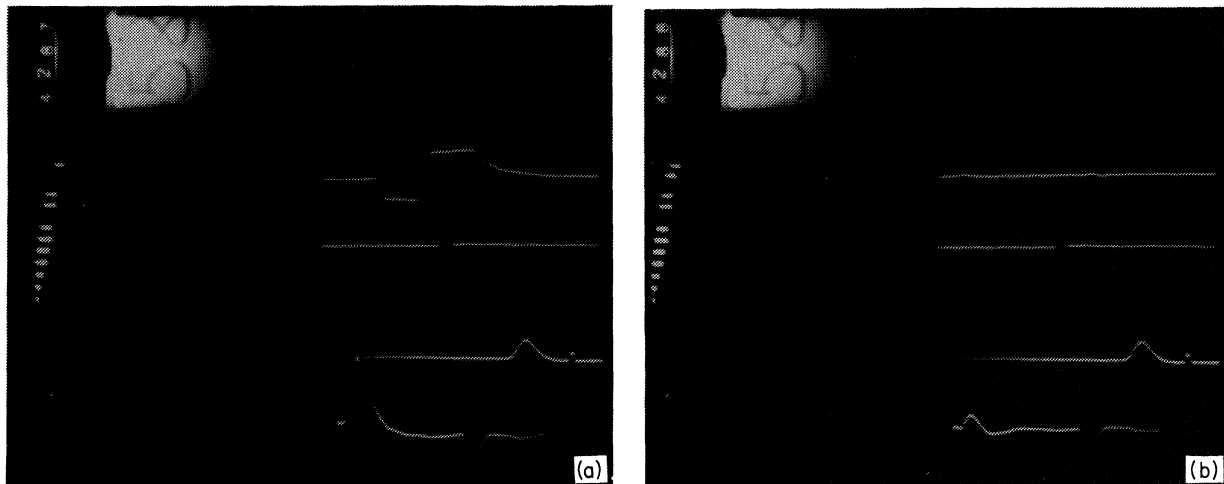

FIG. 11. Photogram of two events on the oscilloscope display. On the two upper tracks of each event, the signals from counters β and γ are displayed. On the third track, one sees some time reference pulses. On the fourth one, the AN_i and TN_i signals from the neutron counter are displayed (left and right pulses, respectively) together with one more time reference signal (central pulse). The numbers and the system of lamps on the left of the pictures refer to the order number of the event: (a) bad event; (b) good candidate event for further selections (no β and γ signals in the two upper tracks).

logic.

During the measurements, the output pulses of the main coincidence and anticoincidence circuits were stored by a system of scalers, the content of which was recorded every 10^7 MONITOR signals.

The neutrons to be attributed to reaction (2) were selected among the events obtained in the *neutral trigger* runs. These were alternated with measurements performed in the *electron trigger* condition, which supplied — for a given number of monitored muons — the number of decay electrons detected by the chosen electron telescope and coming from muons stopped within the gaseous mixture.

Several auxiliary measurements were carried out to get information on the following points:

(a) Time and energy distribution of neutrons coming from nuclear capture of muons directly stopping in the stainless steel wires of the proportional counters. These data were obtained in a special *neutral trigger* run (*iron run*), switching off one section of the γ proportional counter, and accepting events arriving at early times after the MUSTOP signal.

(b) Time and energy distribution of the accidental neutrons. This was done by a usual technique[9] by adding to the $H_2 + D_2$ gaseous mixture a further contamination of 10^{-3} parts of xenon, and measuring neutral events (*xenon run*). In this condition, in fact, owing to the high rate of the transfer reaction (15) in the case $_zY$ = xenon,[24, 23] all the muons which had formed μd atoms were transferred to xenon atoms in a very short time, and were then quickly subject to nuclear capture. The *xenon run* was carried out also in the *electron trigger* condition, to check that the electrons counted in the normal electron runs were actually coming from muons stopped in the gas.

(c) Loss in efficiency for counting electrons, due to the bias conditions of the N_i neutron counters and to the materials placed between the N_i counters and the target gas. This was obtained by recording the counting rates of the (A_i, N_i) telescopes in some *electron trigger* runs as a function of the thickness of additional thin absorbers (iron, plastic, and glass) placed between the A_i counters and the target, and by varying the biases applied to the N_i detectors.

(d) Which correction had to be accounted for, due to the fact that the useful volume V' of the target contributing to the counting rate of the (A_i, N_i) telescopes was slightly bigger than V, because of the additional volume of the disconnected γ_i section. To estimate this correction, a special run was made in which the electron yield was measured while all the γ_i counters were switched off (*total electron trigger run*).

III. DATA ANALYSIS

A. Selection of Neutron Events

In order to sort out the events corresponding to a detected neutron from those collected in the *neutral trigger* runs, a first selection was done through the following steps:

(i) The pictures taken during the measurements were repeatedly scanned to select those in which no β or γ anticoincidence pulse was present within a time interval of 50 microseconds on the oscilloscope tracks (see Fig. 11).

(ii) Only those events for which the N_i amplitudes were contained between 0.35 and 2.5 MeV (electron equivalent energies) were retained. The lower threshold was fixed at this value because the contribution to the counting rate due to accidental neutrons and γ rays, and of neutrons coming from the direct capture of muons stopping in the stainless steel wires of the proportional counters, started to be important below this level. Moreover, also the neutron-γ discrimination efficiency of our apparatus began to be poor below 0.35 MeV (see Fig. 6).

(iii) All the events for which the neutron counter pulses located a point in the γ region of the *amplitude-versus-tail* plot of Fig. 6 were rejected.

The time distribution of the neutron events selected with these criteria was then fitted by an expression of the type

$$A + B \exp(-t/\tau_F) + C \exp(-t/\tau_S) \qquad (17)$$

(see Fig. 12), where A, B, and C are adjustable parameters, $\tau_F = 0.2$ microseconds, and $\tau_S = 2.2$ microseconds.

This type of analysis allowed to subdivide further the neutron events in the following groups:

(a) Those showing a flat time behavior [N_a, first term in Eq. (17)] were due to accidental counts. The level of the accidentals was also determined by analyzing the neutron events obtained in the *xenon run*, and good agreement was found between these two estimates.

(b) Those belonging to the fast component [N_F, second term in Eq. (17)] included the neutrons due to nuclear capture by iron[41] of those muons which directly stopped in the wires of the proportional counters. Furthermore, since (as mentioned above) the μp atoms in the gaseous target disappear with a mean lifetime of about 200 nanoseconds, N_F contained also the neutrons due to muon capture by protons in the μp atoms for which reaction (3) did not occur.

(c) Those corresponding to the slow component [N_S, third term in Eq. (17)] contained mainly the neutrons coming from process (2), i.e., our good
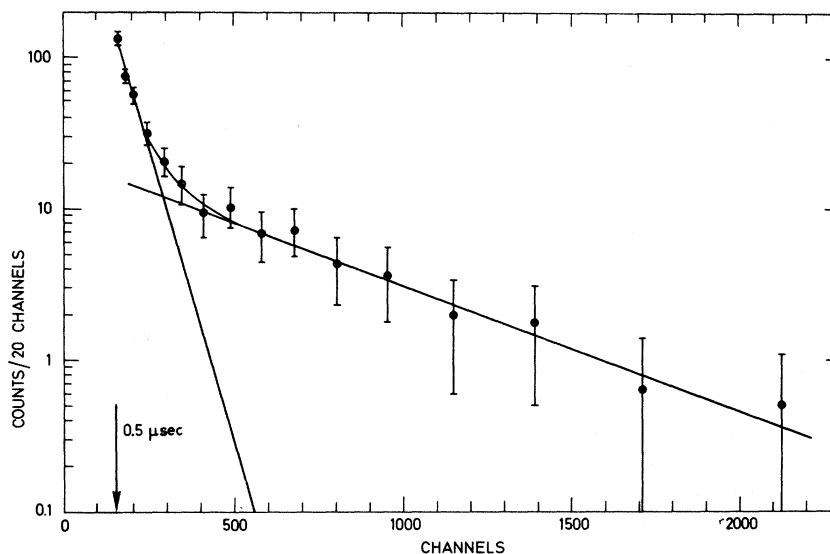
FIG. 12. Experimental time distribution of the neutron events after subtraction of the accidentals. The two straight lines correspond to the two components N_F and N_S, having lifetimes of 0.2 microseconds and 2.2 microseconds, respectively. The arrow shows the time cut used in the analysis. Abscissa: 4.2 nanoseconds/channel.

events, together with the neutrons coming from different processes which the various μ-atomic and μ-molecular systems present in the target may undergo (see Fig. 13). The subtraction of these spurious events will be discussed later on.

From this analysis and with a lower time cut of 0.5 microseconds, we obtained

$$N_a = 233 , \tag{18}$$

$$N_F = 318 , \tag{19}$$

$$N_S = 418 \pm 35 . \tag{20}$$

The total number of accepted[46] MONITOR signals

M^* corresponding to these events was

$$M^*_{tot} = 654.891 \times 10^7 . \tag{21}$$

B. Electron Events

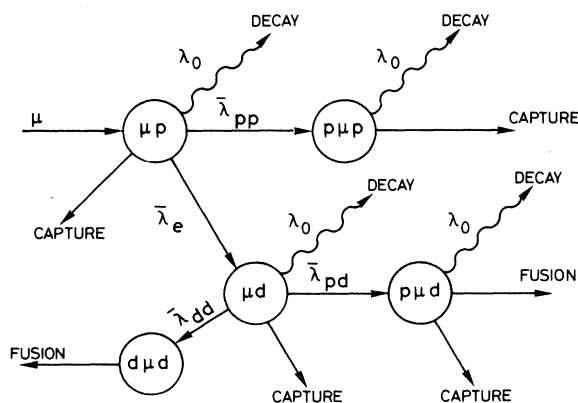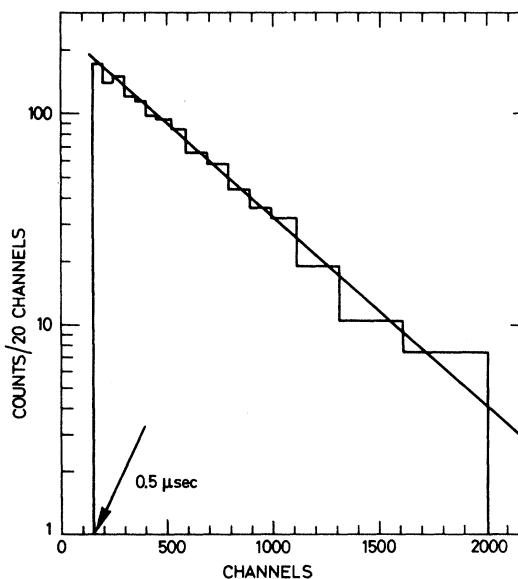The events collected during the *electron trigger* runs were also analyzed in time (see Fig. 14).

FIG. 13. μ-atomic and μ-molecular processes in the gaseous target of deuterated hydrogen. The bars on the rate λ_e, λ_{pp}, λ_{dd}, and λ_{pd} mean that they are to be considered as the effective values referring to the target density and to the chosen deuterium concentration.

FIG. 14. Time distribution of the detected decay electrons coming from muons stopping in the gaseous mixture ($H_2 + 5\%\ D_2$), and corresponding to 2.5×10^7 accepted MONITORS. The straight line represents a lifetime of 2.16 ± 0.14 microseconds. Abscissa: 4.33 nanoseconds/channel.

The level of accidentals was contained within 2%, whereas a small contribution of electrons coming from muons directly stopping in iron was made evident by the *xenon run*.

The number of electrons coming from muons stopped in the useful volume V of the target and detected by our electron telescopes with a lower time cut of 0.5 microsecond was

$$N_{e,t} = 718 \text{ per } 10^7 M^* . \tag{22}$$

To obtain the quantity M to be used in Eq. (16), this number had to be corrected to obtain the number $N_{e,\mu d}$ of detected electrons coming exclusively from μd muonic atoms. This was done assuming for the different atomic and molecular processes shown in Fig. 13 the values given by Bertin et al.[21] (for λ_e), by Dzhelepov et al.[20] (for λ_{dd} and λ_{pd}), and by Bleser et al.[19] (for λ_{pp}) (see Table III). In this way we obtained

$$N_{e,\mu d} = 675 \text{ per } 10^7 M^* . \tag{23}$$

C. Efficiency of Electron Detection

In order to deduce the value $\Lambda_{\exp}$ from Eq. (16), the over-all efficiencies of the apparatus for detecting the neutrons (E) from reaction (2) and for detecting electrons (E_e) were still to be calculated. Special care was put into the evaluation of these quantities, which was performed as described below.

It should be noticed that E_e can be written as

$$E_e = \Omega_e W , \tag{24}$$

where Ω_e is the effective solid angle for the detection of electrons, and W is a factor which takes into account the losses due to both the electronic biases and the materials present between the deuterated hydrogen and the N_i detectors. From the measurements performed with this aim (see Sec. II E), we obtained

$$W = (74 \pm 2)\% \tag{25}$$

in full agreement with the expected value.

The determination of E_e was then reduced to calculate Ω_e. As a first step of the computation, the spatial distribution of the muons stopping in the useful volume V was calculated by a Monte Carlo method. The initial energy and spatial distributions of the beam were known from measurements, and the calculation followed the slowing-down muons through the various collimators and moderators, until they left V or stopped in it.

Only those muons crossing the first grid of the α counter were accepted. The effects due to deviations from the assumed configuration were seen to be very small because of the cylindrical symmetry around the axis of the target of the neutron and electron detectors (see Fig. 3).

The results of this calculation were used as input parameters to calculate Ω_e. This was done including a correction due to the already mentioned fact that, during the *electron trigger* runs, the useful volume V' was slightly bigger than during the *neutron trigger* runs (see Sec. II E). It was obtained that this correction increased the effective solid angle Ω_e by about 8%. This value was confirmed by the measurement in the *total electron trigger* conditions.

The value of Ω_e obtained in this way was

$$\Omega_e = (5.63 \pm 0.11)\% , \tag{26}$$

that is, from Eq. (24),

$$E_e = (4.17 \pm 0.14)\% . \tag{27}$$

D. Efficiency of Neutron Detection

A second Monte Carlo calculation was carried out to evaluate E on the following lines:

(i) Starting from statistics of 10^5 neutrons emitted from the V volume, the number of those arriving at the N_i counters was calculated first. This was done assuming the already calculated spatial distribution of the stopping muons in the region V and the initial energy distribution given by Wang[11] for the neutrons coming from process (2) (see Fig. 1).

The calculation took into account the complete geometry of the apparatus, including the various detectors and shielding materials. The neutron was followed until it had been slowed down to energies lower than 0.05 MeV, or it left the apparatus, or finally entered the detecting volume of one of the N_i counters.

Possible recoil protons which might generate anticoincidence signals in the proportional counters or in the A_i scintillators were also taken into account. The neutrons entering the sensitive volume of the N_i detectors were tagged with their final spatial coordinates and direction of incidence.

(ii) The neutron energy spectrum released from the N_i counters in correspondence of the impinging neutrons was calculated.

Here one must remember that the energy scale and resolution, as well as the biases of the neutron detectors, were provided by the already mentioned calibrations with radioactive sources of γ rays (see Fig. 7). These measurements supplied the response of our neutron counters to electrons in the energy range corresponding to proton energies in the range 0.05–10 MeV. The relative response of the used N_i detectors to electrons and protons in this region of energy was measured separately.[29]
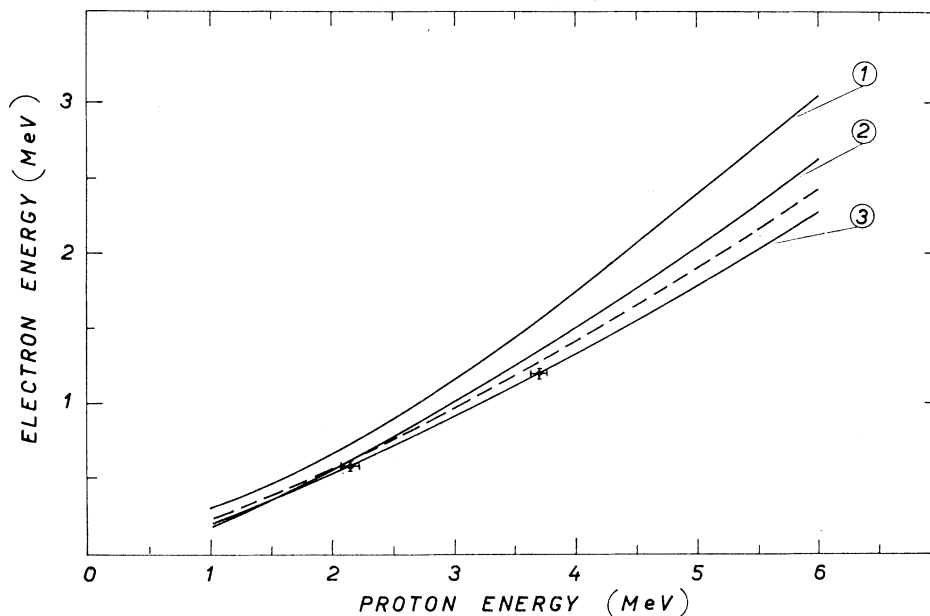
The final neutron energy spectrum from the

FIG. 15. Relative response to electrons and protons of NE-213 liquid scintillators as given by different authors (see Ref. 29). The curve assumed for the present analysis is the response curve 3.

Monte Carlo calculation was then produced in terms of electron equivalent energies, using the measured relative response curve (see Fig. 15).

The 0.35 MeV lower cut used to select the neutron events was finally operated on the theoretical energy distribution. The residual area, divided by the number of initially extracted neutrons, supplied the over-all efficiency E to be used in Eq. (16).

In this way we obtained[47]

$$E = (2.84 \pm 0.18)\% . \tag{28}$$

The quoted error was evaluated by taking into account the excursion of the energy resolution and response curve of the N_i counters within the experimental errors and by varying the main input parameters in the Monte Carlo calculation.

E. Final Corrections to the Neutron Events

To extract from N_S the final number of neutrons due to process (2), one still has to take into account the following contributions (see Fig. 13 and Table VI):

(a) Neutrons coming from muon capture by protons in the $p\mu p$ systems. This correction is practically negligible since the $p\mu p$ molecule forms for about 5×10^{-3} of the stopped muons in our experimental conditions.

(b) Neutrons coming from muon capture by deuterons in the $d\mu d$ ions. This channel is also negligible since, as we already said, this system undergoes the fusion processes (6) and (7) with

high probability.

(c) Neutrons coming from muon capture by protons and deuterons in the $p\mu d$ molecule and by the ^{3}He nucleus produced in the fusion reaction of the $p\mu d$ (see Sec. I B). Such correction was calculated from the quoted values for the rates of the various μ-atomic and μ-molecular processes shown in Fig. 13, and it was found that it contributed to the error on Λ_{exp} for about 2.2%.

(d) Neutrons coming from the fusion reaction (6) in the $d\mu d$ molecule. Assuming the same rates as above, it was found that the correction due to this channel induced an error of about 1% on Λ_{exp}.

(e) Neutrons coming from the delayed diffusion of the μd muonic atoms to the iron wires of the proportional counters. To estimate this background, a Monte Carlo calculation, simulating the counter's geometry, was done, assuming for

TABLE VI. Summary of the different contributions to the total number of selected neutrons.[a]

	N_a	N_F	N_S
Accidentals	233		
Muon nuclear capture:			
by iron		264	87
in μp atoms		54	
in $p\mu d$ ions			24
fusion of $d\mu d$ ions			12
Muon capture in the			
μd atoms			295
Total	233	318	418

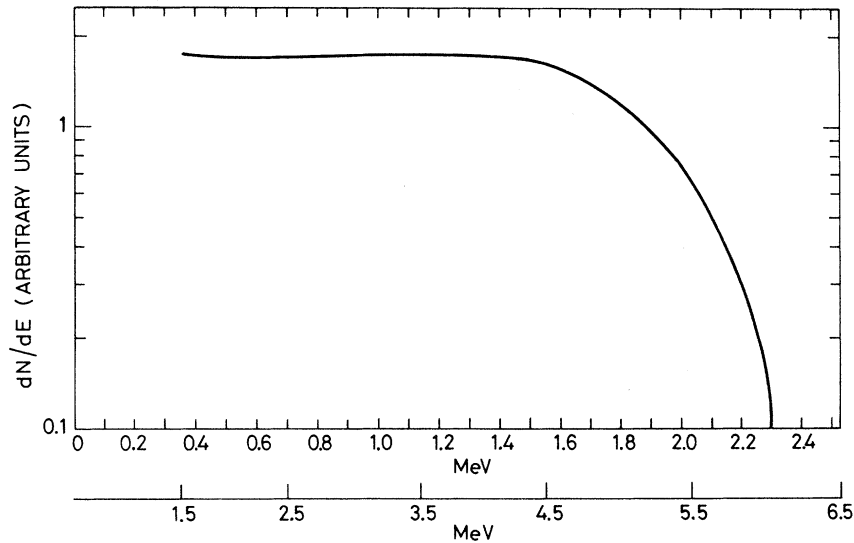[a] See Eqs. (17), (18), (19), and (20).

FIG. 16. Calculated energy spectrum for 5.2-MeV neutrons coming from nuclear capture of muons in μp atoms for the present system of neutron counters. The assumed relative response to electrons and protons was curve 3 in Fig. 15. Abscissas: upper scale: electron equivalent energies; lower scale: proton energies.

the cross sections of process (12) and (13) the experimental results by Dzhelepov et al.,[34] and by Alberigi Quaranta et al.,[30] respectively (see Table IV).

This correction, due to the low-energy spectrum of the neutron we were interested in (see Fig. 1), turned out to be the biggest of all the ones considered. Its influence on the final error on Λ_{exp} was estimated to be 4.5%.

The calculated number of neutrons to be sub-

tracted from N_S due to all of these effects is listed in Table VI. To obtain the values shown in the table, one obviously had to know the efficiency of the apparatus to detect the neutrons emitted in the different processes. The efficiencies were obtained as precedingly described for the neutrons due to process (2), running the Monte Carlo program for each channel (a)–(e) with the proper initial distribution of neutron energies.

From this analysis, the following number of neutrons due to process (2) was finally accepted:

$$N = (295 \pm 27). \qquad (29)$$

The quoted error on N includes also the uncertainty with which the various background contributions listed in Table VI are known.

Figures 16 and 17 show the Monte Carlo calculated energy spectra for our system of counters in the case of the 5.2-MeV neutrons coming from nuclear capture of muons in hydrogen, and of the 3.3-MeV neutrons from the fusion reaction (6) in the $d\mu d$ ions. Figure 18 shows the experimental neutron energy spectrum obtained in a single *iron run*. The energy distribution of the accidental neutrons showed a typical evaporative spectrum.

Figure 19 shows the energy spectrum of the 295 neutrons attributed to reaction (2). The background counts of the various kinds listed in Table VI are subtracted in the figure after proper normalization. The solid line represents the result of the Monte Carlo calculation when the initial energy distribution for the extracted neutrons was assumed equal to that of Wang.[11]
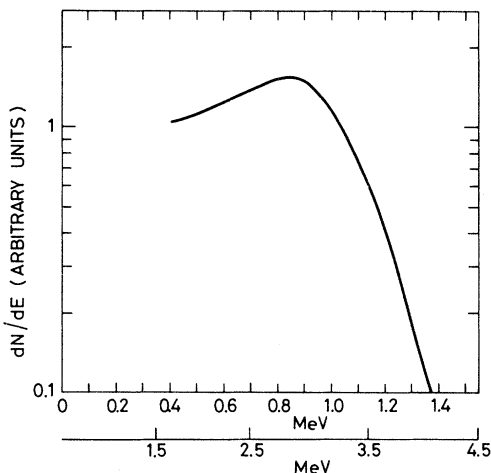

FIG. 17. Calculated energy spectrum for 3.3-MeV neutrons coming from the fusion reaction in the $d\mu d$ molecular ions. The calculation assumed the relative response curve to electrons and protons as given by curve 3 in Fig. 15. Abscissas: upper scale: electron equivalent energies; lower scale: proton energies.
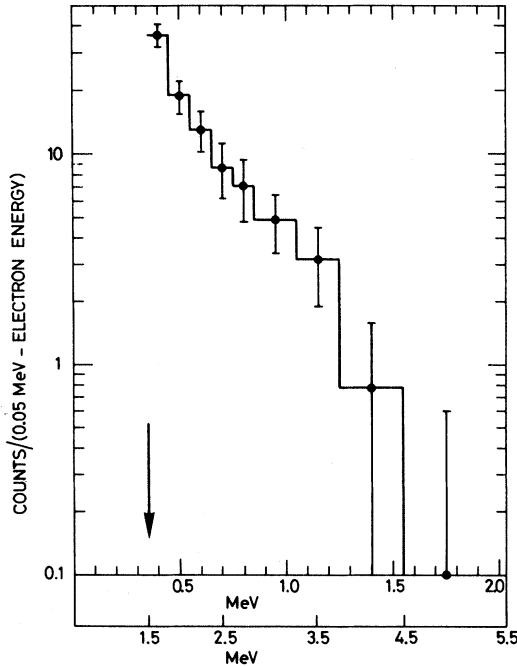
FIG. 18. Energy distribution of the pulses due to neutrons coming from muon capture in iron nuclei, as measured during the *iron run*. Abscissas: upper scale: electron equivalent energies; lower scale: proton energies. The arrow shows the low-energy cut used during the analysis.
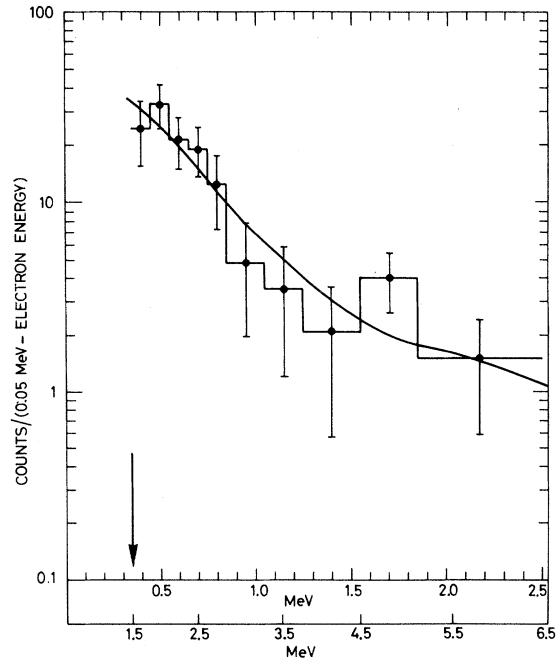

FIG. 19. Experimental energy spectrum of the pulses due to the 295 neutrons coming from muon capture by deuterons in the μd muonic atoms. The low-energy cut effected in the analysis is shown by the arrow. The solid line represents the expected amplitude spectra (normalized to the number of events) calculated by the Monte Carlo method starting from the theoretical neutron energy spectrum shown in Fig. 1. Abscissas: upper scale: electron equivalent energies; lower scale: proton energies.

IV. RESULTS AND CONCLUSIONS

The main results of the measurements and of the analysis described in the previous sections are $N = 295 \pm 27$, $E = (2.84 \pm 0.18)\%$, $N_{e,\mu d} = 442\,209$, $E_e = \Omega_e W = (4.17 \pm 0.14)\%$. From these values, setting $M = N_{e,\mu d}/E_e$ in Eq. (16), one gets

$$\Lambda_{\exp} = (445 \pm 60)\ \sec^{-1}, \tag{30}$$

where the error is calculated by adding quadratically the errors given in the above list.

To check the consistency of this result against possible biases introduced by the analysis, the data were processed using different combinations of time and energy cuts. From Table VII it can be seen that the experimental result given by Eq. (30) is dependent in a negligible way on the choice of these thresholds.

We can now draw the following conclusions:

(i) Referring to Table II, one sees that the present result (30) is in fair agreement with the theoretical predictions referring to the capture rate Λ_d in the doublet state of the muon-deuteron system, whereas it is inconsistent with the expectation value for the rate Λ_{st} referring to a statistical mixture of quartet and doublet state.

As was previously said, however, little infor-

mation is available on the final spin state of the μd atoms in our target. For the present, then, we shall conclude that the result given by Eq. (30) supports the suggestion[28] that the nuclear capture occurs mostly from the doublet spin state of the μd atoms in the present conditions.

(ii) The value given by Eq. (30) is then in agreement with the preceding experimental result by Wang,[15]

$$\Lambda_d = (365 \pm 96)\ \sec^{-1}, \tag{31}$$

which refers to muon capture by deuterons proceeding from the doublet state.

(iii) In Fig. 20 the dependence of Λ_d on the ratio $g_{A,\mu}/g_{V,\mu}$ is given as obtained starting from the calculation by Wang[11]; the full line in the figure was calculated assuming for the ratio $g_{P,\mu}/g_{V,\mu}$ the value supplied by the one-pion exchange dominance,[48] i.e.,

$$\frac{g_{P,\mu}}{g_{V,\mu}} = -\frac{4g_{\pi nn}}{m_\pi^2 - q^2}\left(\frac{\pi}{m_\pi^2 \tau_\pi}\right)^{1/2}\left(1 - \frac{m_\mu^2}{m_\pi^2}\right)^{-1}\frac{1}{g_{V,\mu}}$$

$$= -9.1, \tag{32}$$

TABLE VII. Values of Λ_{exp} obtained in the present work for different choices of energy and time lower thresholds.[a]

Time cut (μ sec)	Energy cut (MeV-electron energies)	Λ_{exp} (sec^{-1})
0.5	0.35	445
0.5	0.45	443
0.8	0.35	429
0.8	0.45	447

[a]The errors on the values of Λ_{exp} presented in the table due to the fitting procedure are between 8% and 12%.

where $g_{\pi nn}$ is the pion-nucleon coupling constant, m_π and m_μ are the masses of the pion and of the muon, respectively, τ_π is the pion lifetime, and $q^2 = -0.88\, m_\mu^2$.[2]

The two experimental results (30) and (31) are also represented in Fig. 20; if one combines them, one gets

$$\overline{\Lambda}_{exp} = (424 \pm 56)\ \text{sec}^{-1}, \tag{33}$$

which leads, according to the graph of Fig. 20, to the value

$$\frac{g_{A,\mu}}{g_{V,\mu}} = -(1.35 \pm 0.10). \tag{34}$$

We remind here that, since process (2) is an almost pure Gamow-Teller transition, Λ_d depends rather weakly both on $g_{P,\mu}$ and on $g_{M,\mu}$; therefore, no significant variation of the result given by Eq. (34) would be obtained in correspondence to small deviations from the assumed value (32) for $g_{P,\mu}/g_{V,\mu}$. As to the validity of such an assumption, one should keep in mind that the experimental results on muon capture by hydrogen[9] and by heavier nuclei (like ^{3}He, ^{12}C, and ^{16}O; see, for instance, Ref. 17) are all consistent with Eq. (32); however, no independent experimental evidence exists, proving that $g_{P,\mu}/g_{V,\mu}$ is not much different from the value (32).

(iv) As a final remark, we should like to mention that the value given by Eq. (34) for $g_{A,\mu}/g_{V,\mu}$ is in agreement with the results on the same ratio obtained from neutron decay,[49-51] as required
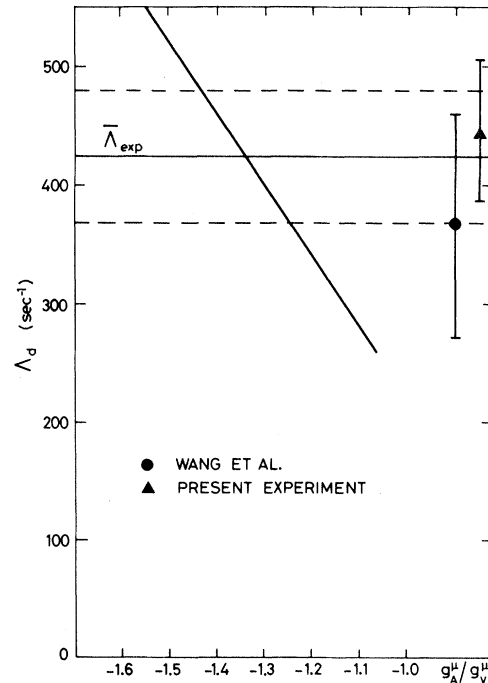

FIG. 20. Theoretical dependence of the nuclear capture rate of muons by deuterons in the doublet state of the muon-deuteron system (Λ_d) on the ratio $g_{A,\mu}/g_{V,\mu}$, obtained assuming $g_{P,\mu}/g_{V,\mu} = -9.1$, $a_{nn} = -16.4$ F, and $r_{0,nn} = 2.8$ F. Also shown in the figure are the results obtained in the present work and in the experiment by Wang et al. (see Ref. 15) on the nuclear capture rate of muons by deuterons, together with their average value ($\overline{\Lambda}_{exp}$).

by muon-electron universality (universal Fermi interaction).

*Now at CERN.
†Work partially supported by the Third Committee of the INFN.
[1]H. Primakoff, Rev. Mod. Phys. 31, 802 (1959); J. Bernstein, T. D. Lee, C. N. Yang, and H. Primakoff, Phys. Rev. 111, 313 (1958).
[2]S. Weinberg, Phys. Rev. Lett. 4, 585 (1960); A. Halpern,

Phys. Rev. 135, A34 (1964); P. K. Kabir, Z. Phys. 191, 447 (1966).
[3]A. Fujii, Nuovo Cimento 27, 1025 (1963); 42, 109 (1966).
[4]P. Pascual, CERN Report No. TH 1081, 1969 (unpublished).
[5]R. Hildebrand, Phys. Rev. Lett. 8, 34 (1962); R. Hildebrand and J. H. Doede, in Proceedings of the Inter-

national Conference on High-Energy Physics at CERN,
edited by J. Prentki (CERN, Geneva, 1962), p. 418;
J. H. Doede and R. Hildebrand, cited by C. Rubbia, in
Proceedings of the International Conference on Funda-
mental Aspects of Weak Interactions (Brookhaven
National Laboratory, Upton, New York, 1964), p. 277.

[6]E. J. Bleser, L. M. Lederman, J. L. Rosen, J. E.
Rothberg, and E. Zavattini, Phys. Rev. Lett. $\underline{8}$, 288
(1962).

[7]E. Bertolini, A. Citron, G. Gialanella, S. Focardi,
A. Mukhin, C. Rubbia, and F. Saporetti, in *Proceed-*
ings of the International Conference on High-Energy
Physics at CERN, edited by J. Prentki (CERN, Geneva,
1962), p. 421.

[8]J. E. Rothberg, E. W. Anderson, E. J. Bleser, L. M.
Lederman, S. L. Meyer, J. L. Rosen, and I-T. Wang,
Phys. Rev. $\underline{132}$, 2664 (1963).

[9]A. Alberigi Quaranta, A. Bertin, G. Matone, F. Pal-
monari, G. Torelli, P. Dalpiaz, A. Placci, and
E. Zavattini, Phys. Rev. $\underline{177}$, 2118 (1969).

[10]H. Überall and L. Wolfenstein, Nuovo Cimento $\underline{10}$, 136
(1958).

[11]I-T. Wang, Phys. Rev. $\underline{139}$, B1539 (1965).

[12]E. Cremmer, Nucl. Phys. $\underline{B2}$, 409 (1967).

[13]P. Pascual, R. Tarrach, and F. Vidal, Nuovo Cimento
$\underline{11A}$, 241 (1972).

[14]E. Truhlik, Nucl. Phys. $\underline{B45}$, 303 (1972).

[15]I-T. Wang, E. W. Anderson, E. J. Bleser, L. M. Leder-
man, S. L. Meyer, J. L. Rosen, and J. E. Rothberg,
Phys. Rev. $\underline{139}$, B1528 (1965).

[16]E. Cremmer, private communication.

[17]E. S. Burhop, *Mesonic Atoms in High Energy Physics*
(Academic, New York, 1969), Vol. 3; Y. N. Kim,
Mesic Atoms and Nuclear Structure (North-Holland,
Amsterdam, 1971); E. Zavattini (to be published in
Muon Physics).

[18]G. Conforto, C. Rubbia, E. Zavattini, and S. Focardi,
Nuovo Cimento $\underline{33}$, 1001 (1964).

[19]E. J. Bleser, E. W. Anderson, L. M. Lederman, S. L.
Meyer, J. L. Rosen, J. E. Rothberg, and I-T. Wang,
Phys. Rev. $\underline{132}$, 2679 (1963).

[20]V. Dzhelepov, P. F. Ermolov, V. I. Moskalev, and V. V.
Fil'chenkov, Zh. Eksp. Teor. Fiz. $\underline{50}$, 1235 (1966)
[Sov. Phys.—JETP $\underline{23}$, 820 (1966)].

[21]A. Bertin, M. Bruno, V. Vitale, A. Placci, and
E. Zavattini, Nuovo Cimento Lett. $\underline{4}$, 449 (1972).

[22]A. Placci, E. Zavattini, A. Bertin, and A. Vitale,
Nuovo Cimento $\underline{A64}$, 1053 (1969).

[23]A. Bertin, M. Bruno, A. Vitale, A. Placci, and
E. Zavattini, Phys. Rev. A $\underline{7}$, 462 (1973).

[24]A. Placci, E. Zavattini, A. Bertin, and A. Vitale,
Nuovo Cimento $\underline{A52}$, 1274 (1967).

[25]E. Di Capua, R. Garland, L. Pondrom, and A. Streiz-
off, Phys. Rev. $\underline{133}$, B1333 (1964).

[26]See, for example, E. J. Maier, R. M. Edelstein, and
R. T. Siegel, Phys. Rev. $\underline{133}$, B663 (1964).

[27]L. L. Foldy and J. D. Walecka, Phys. Rev. $\underline{140}$, B1339

(1965).

[28]A. Placci, E. Zavattini, A. Bertin, and A. Vitale,
Phys. Rev. Lett. $\underline{25}$, 475 (1970).

[29]A. Bertin, A. Vitale, and A. Placci, Nucl. Instrum.
Methods $\underline{91}$, 649 (1971).

[30]A. Alberigi Quaranta, A. Bertin, G. Matone, F. Pal-
monari, A. Placci, P. Dalpiaz, G. Torelli, and
E. Zavattini, Nuovo Cimento $\underline{B47}$, 72 (1967).

[31]S. Cohen, D. L. Judd, and R. J. Riddell, Phys. Rev.
$\underline{119}$, 397 (1960).

[32]Y. B. Zel'dovich and S. S. Gershtein, Usp. Fiz. Nauk
$\underline{71}$, 581 (1961) [Sov. Phys.—Usp. $\underline{3}$, 593 (1961)].

[33]A. V. Matveenko, and L. I. Ponomarev, Zh. Eksp.
Teor. Fiz. $\underline{59}$, 1593 (1970) [Sov. Phys.—JETP $\underline{32}$, 871
(1971)].

[34]V. P. Dzhelepov, P. F. Ermolov, V. I. Moskalev, and
V. V. Fil'chenkov, Zh. Eksp. Teor. Fiz. $\underline{50}$, 1235
(1966) [Sov. Phys.—JETP $\underline{23}$, 820 (1966)].

[35]V. P. Dzhelepov, P. F. Ermolov, V. I. Moskalev,
V. V. Fil'chenkov, and M. Friml, Zh. Eksp. Teor. Fiz.
$\underline{47}$, 1243 (1964) [Sov. Phys.—JETP $\underline{20}$, 841 (1965)].

[36]J. H. Doede, Phys. Rev. $\underline{132}$, 1782 (1963).

[37]See E. Fermi, Z. Phys. $\underline{60}$, 320 (1930).

[38]S. S. Gershtein, Zh. Eksp. Teor. Fiz. $\underline{40}$, 698 (1961)
[Sov. Phys.—JETP $\underline{13}$, 488 (1961)].

[39]V. B. Belyaev, S. S. Gershtein, B. N. Zakharev, and
S. P. Lomnev, Zh. Eksp. Teor. Fiz. $\underline{37}$, 1652 (1959)
[Sov. Phys.—JETP $\underline{10}$, 1171 (1960)].

[40]A. Bertin, A. Vitale, and A. Placci, Nucl. Instrum.
Methods $\underline{68}$, 24 (1969).

[41]J. C. Sens, Phys. Rev. $\underline{113}$, 679 (1959).

[42]Supplied by Engelhard Industries, Newark, New Jersey.

[43]Supplied by Air Liquide, Paris, France.

[44]A. Alberigi Quaranta, A. Bertin, G. Matone, F. Pal-
monari, A. Placci, P. Dalpiaz, and E. Zavattini, Nucl.
Instrum. Methods $\underline{55}$, 273 (1967).

[45]The glass cells filled with the NE-213 liquid were
specially made by Nuclear Enterprise, Ltd., Sighthill,
Edinburgh, Scotland.

[46]An acceptance circuit was operating in the electronics
in such a way so as to eliminate accidental counts
following one MONITOR signal and due to those muons
which previously entered the apparatus (see Ref. 9).

[47]The presented value for E includes the fact that two
neutrons are emitted in process (2). Also the kinemati-
cal correlation due to the final-state interaction be-
tween the two neutrons was taken into account.

[48]L. Wolfenstein, Nuovo Cimento $\underline{8}$, 882 (1958).

[49]C. J. Christensen, A. Nielsen, A. Bahnsen, W. K.
Brown, and B. M. Rustad, Phys. Lett. $\underline{26B}$, 11 (1967).

[50]C. J. Christensen, V. E. Krohn, and G. R. Ringo, Phys.
Rev. C $\underline{1}$, 1693 (1970).

[51]For a critical study of possible renormalization of g_A
in nuclei, see D. H. Wilkinson, Phys. Rev. C $\underline{7}$, 930
(1973); and M. Ericson, Figureau, and C. Thevenet,
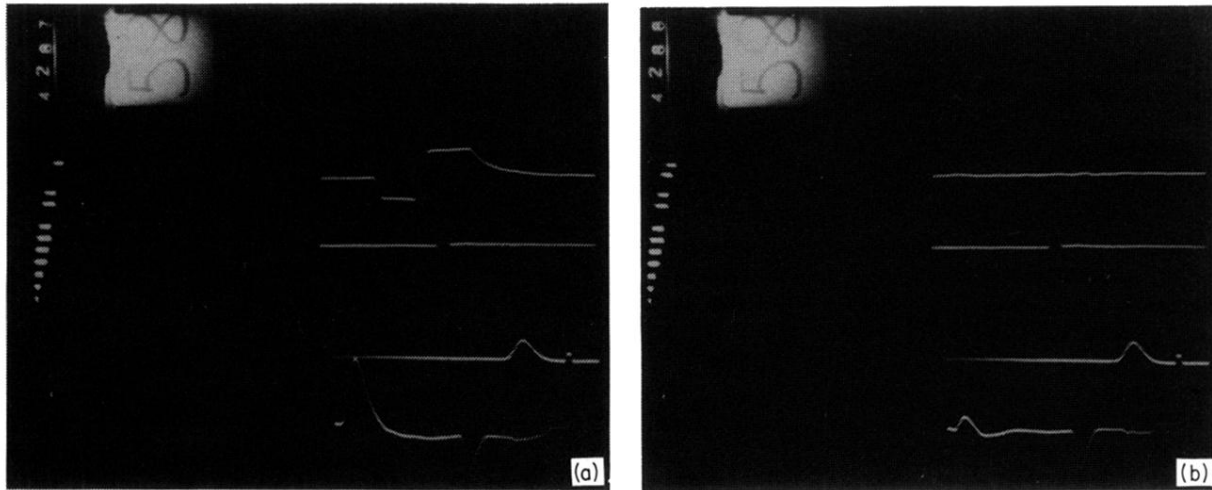Report No. LYCEN 73-17, 1973 (unpublished).

FIG. 11. Photogram of two events on the oscilloscope display. On the two upper tracks of each event, the signals from counters β and γ are displayed. On the third track, one sees some time reference pulses. On the fourth one, the AN_i and TN_i signals from the neutron counter are displayed (left and right pulses, respectively) together with one more time reference signal (central pulse). The numbers and the system of lamps on the left of the pictures refer to the order number of the event: (a) bad event; (b) good candidate event for further selections (no β and γ signals in the two upper tracks).